AIAA JOURNAL
Vol. 38, No. 7, July 2000

Computational Fluid Dynamics Algorithms for Unsteady Shock-Induced Combustion, Part 2: Comparison

Jeong-Yeol Choi*
Pusan National University, Pusan 609-735, Republic of Korea
and
In-Seuck Jeung† and Youngbin Yoon*
Seoul National University, Seoul 151-742, Republic of Korea

In addition to the validation of the baseline method (Choi, J.-Y., Jeung, I.-S., and Yoon, Y., "Computational Fluid Dynamics Algorithms for Unsteady Shock-Induced Combustion, Part 1: Validation," *AIAA Journal*, Vol. 38, No. 7, 2000, pp. 1179–1187), numerical experiments were performed to investigate the characteristics of various numerical algorithms for the analysis of periodically unstable shock-induced combustion. With regard to the spatial discretization, the role of limiter functions and entropy-fixing parameters were examined concerning inherent artificial damping. Instead of the Roe scheme, an advection upstream splitting method variant upwind scheme was applied to the present problem and compared with the baseline method. Next, the accuracy and efficiency of time-integration approaches were tested by carrying out time-step refinement studies. A four-step explicit Runge–Kutta method, a point-implicit method, a Crank–Nicolson method, and a dual-time-stepping method were considered in addition to the baseline method.

Introduction

As mentioned in this paper's companion study,[1] there have been a number of computational studies on shock-induced combustion. Although all of the previous studies were carried out under validation conditions through general comparisons with experimental data, there are a wide variety of computational methods with which to do so. Wilson and Sussman used a point-implicit time integration and compared a modified Steger–Warming flux vector splitting with an upwind total variation diminishing (TVD) scheme.[2] Matsuo et al. used a non-MUSCL TVD scheme with explicit time integration.[3] Ahuja et al.[4] used a shock-fitting technique and a McCormack scheme instead of the widely used TVD-type shock-capturing schemes. Recently, Yungster and Radhakrishnan developed a time-accurate fully implicit TVD code for unsteady shock-induced combustion calculations.[5]

In those studies, Yee's TVD schemes[6] based on Roe's flux difference splitting[7] (FDS) were widely used for spatial discretization, but various time-integration methods ranging from an explicit scheme to a fully implicit scheme were applied. However, it is difficult to find an accurate and efficient method for the study of unsteady shock-induced combustion or related phenomena because a comparative study of numerical algorithms for shock-induced combustion or relevant problems is rarely found. Even though there are some comparative studies of computational algorithms for steady nonreactive gas flows in supersonic or hypersonic range,[6,8] it is hard to adopt the guidelines from the steady nonreactive flow studies for unsteady reactive gas flows. Hence, this study aims at providing a reference for computational studies of shock-induced combustion and related supersonic combustion phenomena by presenting comparative results of various computing algorithms used for the simulation of unsteady shock-induced combustion.

The present study is based on the development and validation of a baseline fully implicit TVD scheme described in Ref. 1. In this code, Roe's FDS[7] and MUSCL-type TVD extension were used for the spatial discretization of governing equations, and a second-order-accurate fully implicit lower-upper (LU) relaxation scheme was used for the time integration with a Newton subiteration method. The effects of the different choices of computational algorithms were investigated within the following two categories, spatial discretization and time integration. In the section on spatial discretization, the role of limiter functions and entropy-fixing parameters were investigated by comparing the oscillation frequency of pressure history at the stagnation point. In this category, a variant of the advection upstream splitting method (AUSM),[9] newly used for shock-induced combustion studies[10,11] was also applied for the simulation of oscillatory shock-induced combustion and was compared with the Roe's FDS method.[7] With regard to time integration, four different time-integration schemes were used in addition to the baseline method. The considered methods are an explicit four-step Runge–Kutta (RK) method,[12] a point-implicit (PI) method,[13] a fully implicit Crank–Nicolson (CN) method,[12] and a dual-time-stepping method.[14] In this category, the time accuracy and solution efficiency was compared through a time step refinement study for each scheme.

Baseline Computational Modeling

Because the detailed description of governing equations and baseline numerical methods are addressed in Ref. 1, they will be only briefly repeated in this section for the comparison and description of other numerical methods in the following sections. The Euler equations for reactive flows are written in the following vector form in a curvilinear coordinate:

$$\frac{\partial \boldsymbol{Q}}{\partial t} + \frac{\partial \boldsymbol{F}}{\partial \xi} + \frac{\partial \boldsymbol{G}}{\partial \eta} + \boldsymbol{H} = \boldsymbol{W} \tag{1}$$

Here $\boldsymbol{Q}$ is a conservative variable vector, $\boldsymbol{F}$ and $\boldsymbol{G}$ are flux vectors in the generalized coordinate ξ and η directions, $\boldsymbol{H}$ is an axisymmetric term, $\boldsymbol{W}$ is a chemical source vector, and t is time. Chemistry modeling of the equations will be omitted here because it is addressed in detail in Ref. 1.

By applying the Newton-iteration method to a second-order time-accurate formulation, the governing equations is discretized as the following fully implicit formulation:

$$\left(c_0\boldsymbol{I} - \left(\frac{\partial \boldsymbol{R}}{\partial \boldsymbol{Q}}\right)\right)^{n+1,m}_{i,j} \Delta \boldsymbol{Q}^{n+1,m}_{i,j} = -c_0\boldsymbol{Q}^{n+1,m}_{i,j} - c_1\boldsymbol{Q}^{n}_{i,j} - c_2\boldsymbol{Q}^{n-1}_{i,j} + \boldsymbol{R}\left(\boldsymbol{Q}^{n+1,m}_{i,j}\right) \tag{2}$$

Here, n is the time step; m is the subiteration level at every time step; c_0, c_1, and c_2 are the coefficients from the variable time step size;

Presented as Paper 98-3217 at the AIAA/ASME/SAE/ASEE 34th Joint Propulsion Conference, Cleveland, OH, 13–15 July 1998; received 14 January 1999; revision received 13 December 1999; accepted for publication 29 December 1999.

*Assistant Professor, Department of Aerospace Engineering. Member AIAA.
†Professor, Department of Aerospace Engineering. Senior Member AIAA.

and $\boldsymbol{R}$ is the residual vector discretized by finite volume formulation as follows:

$$\boldsymbol{R}_{i,j} = \boldsymbol{W}_{i,j} - \boldsymbol{H}_{i,j} - \tilde{\boldsymbol{F}}_{i+\frac{1}{2},j} + \tilde{\boldsymbol{F}}_{i-\frac{1}{2},j} - \tilde{\boldsymbol{G}}_{i,j+\frac{1}{2}} + \tilde{\boldsymbol{G}}_{i,j-\frac{1}{2}} \quad (3)$$

$\boldsymbol{W}$ and $\boldsymbol{H}$ are evaluated at each grid point (i, j), and $\tilde{\boldsymbol{F}}$ and $\tilde{\boldsymbol{G}}$ are the numerical fluxes evaluated at cell interfaces. The numerical fluxes are flux vectors containing artificial damping and are formulated by appropriate spatial discretization schemes such as Roe's FDS.[7] At every subiteration step, the conservative variables are updated by calculating the variation of conservative variables from Eq. (2). The implicit formulation in Eq. (2) is a pentadiagonal system, and the baseline method solves this equation by an LU relaxation scheme.[15]

Spatial Discretization

Generally, the spatial discretization deals with the formulation of numerical flux in Eq. (3), and the basic difference of the flux formulations comes from the different treatment of artificial damping. Although there are various central and upwind difference schemes having their own artificial damping characteristics, Roe's FDS scheme[7] seems to be the prevailing one, at least for problems similar to the one discussed here.[2,3,5–8] The higher-order extension of Roe's FDS results in a number of variants that show different shock capturing characteristics according to their inherent artificial damping.[6] However, it is hard to quantify the magnitude of the artificial damping because it acts selectively or nonlinearly in cases where damping is needed. The artificial damping is controlled by a nonlinear function of variable gradient, a so-called limiter. Hence, each numerical flux formulation algorithm shows different damping characteristics according to its limiter function. Therefore, this section deals with the characteristics of spatial discretization schemes with the focus on the role of artificial damping on the oscillatory combustion characteristics.

All of the following examinations were made for a Lehr's experimental case[16] of Mach number 4.48 with a 200×300 grid and initial and boundary conditions described in Ref. 1. The same baseline computational method was used for each case, but the first-order time integration was applied without subiterations for computational efficiency and for clear comparison without the corruption of a pressure history by high-frequency oscillations. Except for the conditions just cited, all of the computational conditions were the same as in the baseline method.[1]

Effect of Spatial Limiter Functions

The most distinctive characteristics of different limiter functions would be the shock-capturing characteristics originating from generic numerical diffusivity. As an example, the minmod limiter shows the most diffusive solution with $\beta = 1.0$ and the steepest one with $\beta = 4.0$ for a third-order scheme in the TVD region. Here, β is a high-order extension parameter for the MUSCL scheme.[1] Instead of the minmod limiter used in the baseline method,[1] other limiter functions can also be used. In this study, Koren's limiter (see Ref. 17) and the so-called van Albada's differentiable limiter (see Ref. 18) functions are considered. In the case of Koren's limiter (see Ref. 17), variables are interpolated at cell interfaces as

$$q_L = q_i + \frac{s}{4}\left[(1-\eta)\delta_{i-\frac{1}{2}} + (1+\eta)\delta_{i+\frac{1}{2}}\right]$$

$$q_R = q_{i+1} - \frac{s}{4}\left[(1+\eta)\delta_{i+\frac{1}{2}} + (1-\eta)\delta_{i+\frac{2}{3}}\right]$$

$$s = \frac{3\Delta\nabla + \varepsilon}{2(\Delta - \nabla)^2 + 3\Delta\nabla + \varepsilon}, \quad \varepsilon \le 1.0 \times 10^{-6} \quad (4)$$

In case of van Albada's limiter (see Ref. 18), variables are interpolated at cell interfaces as

$$q_L = q_i + \frac{s}{4}\left[(1-s\eta)\delta_{i-\frac{1}{2}} + (1+s\eta)\delta_{i+\frac{1}{2}}\right]$$

$$q_R = q_{i+1} - \frac{s}{4}\left[(1+s\eta)\delta_{i+\frac{1}{2}} + (1-s\eta)\delta_{i+\frac{2}{3}}\right]$$

$$s = \frac{2\Delta\nabla + \varepsilon}{\Delta^2 - \nabla^2 + \varepsilon}, \quad \varepsilon \le 1.0 \times 10^{-6} \quad (5)$$

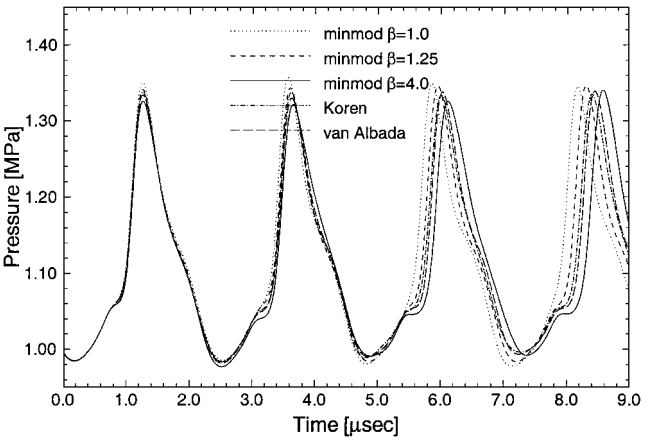

Fig. 1 Temporal variations of pressure at stagnation point for different limiter functions and first-order time integration of 1000 time steps.

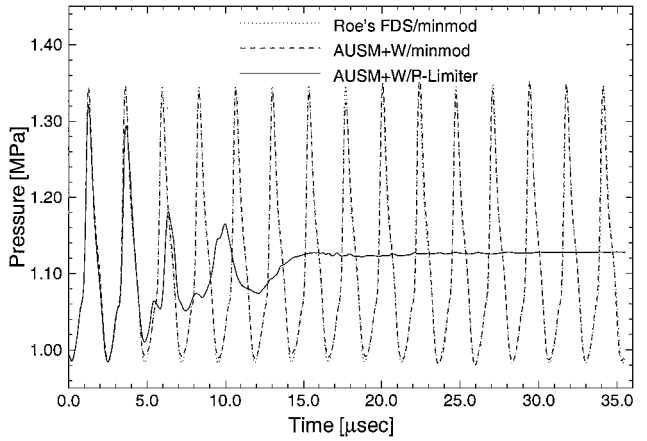

Fig. 2 Temporal variations of pressure at stagnation point for different limiter functions and first-order time integration of 4000 time steps.

These differentiable limiter functions are slightly more efficient than minmod functions because they do not need logical operations such as min and max. They showed the shock-capturing characteristics between minmod with $\beta = 1.0$ and 4.0, although the Koren's limiter (see Ref. 17) also showed a more diffusive solution.

Computation was carried out with four different limiter functions, minmod with $\beta = 1.0$, minmod with $\beta = 4.0$, Koren's limiter (see Ref. 17), and van Albada's limiter (see Ref. 18) in addition to the baseline solution of minmod with $\beta = 1.25$. The results were compared via the stagnation pressure history for the understanding of the effect of artificial damping on oscillatory characteristics. In the resulting pressure history (Fig. 1), the most distinguishing feature of the solution is the phase shift of the oscillatory pressure wave. The steepest limiter (minmod with $\beta = 4.0$) shows the longest period of oscillation, and the most diffusive limiter (minmod with $\beta = 1.0$) shows the shortest period. Because other limiter functions have intermediate shock-capturing characteristic between the two aforementioned limiter functions, they show intermediate solutions.

To find the change of oscillation frequency more precisely, the time integration has been carried out for a longer time to include more oscillation periods. Figure 2 is the pressure history obtained after 4000 steps of time integration. The resulting oscillation frequencies are obtained from this pressure history. Figure 2 includes 15–16 periods of oscillation, and the oscillation frequency is evaluated from the average of the time from the first peak to the last peak and the time from the first valley to the last valley divided by the number of periods. Table 1 shows the resulting oscillation frequencies for the different limiter functions. As listed in Table 1, the steep limiter results in low frequency and the diffusive limiter results in high frequency. The maximum deviation is about 11 kHz corresponding to a 2.5% error in frequency. The experimental result is within the deviation. Therefore, it is understood that the result of

Table 1 Comparison of the oscillation frequency for different limiter functions

Limiter function	Frequency, kHz
Experiment	425
Yungster and Radhakrishnan[5]	431
Minmod, β = 1.00	429.48
Minmod, β = 1.25	426.13
Minmod, β = 4.00	418.73
Koren (see Ref. 17)	423.19
van Albada (see Ref. 18)	421.78

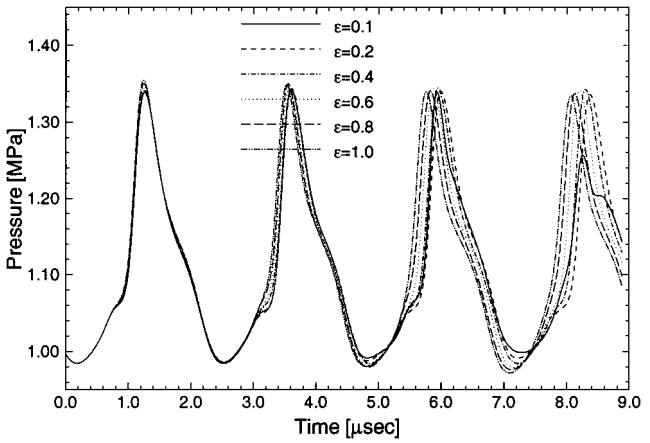

Fig. 3 Temporal variations of pressure at stagnation point with respect to the different values of entropy-fixing parameter in Eq. (38) of Ref. 1.

numerical simulation could have some deviation originating from the choice of spatial discretization method, each having its own inherent numerical dissipation. The computing times of Koren's limiter (see Ref. 17) and van Albada's limiter (see Ref. 18) were slightly better than those of the minmod limiter, but the selection of limiter function had a negligible influence on overall computing time because the largest part of the computing time is consumed by the matrix inversion of the implicit part.

Entropy-Fixing Parameter

Many of the FDS-type upwind schemes have entropy problems such as carbuncle, expansion shock waves, and even–odd decoupling. Some kinds of entropy fix are used to avoid this problem, but the quantity of entropy fix also influences artificial dissipation, shock thickness, and the convergence rate because it modifies the magnitude of eigenvalues relevant to the quantity of artificial damping.[19] However, there is no rule of thumb for determining the entropy parameter, a small number $\tilde{\varepsilon}$ in Eq. (38) of Ref. 1, although this parameter is typically recommended to be in the range of $0.01 \leq \tilde{\varepsilon} \leq 0.1$ for most of the problems.[19] Especially in a hypersonic problem, it is known that the small range of numbers just given does not cure the convergence problem, and a much larger value is used often, although the use of large value is avoided for the validity problem. Thus, in addition to the baseline solution with $\tilde{\varepsilon} = 0.4$, some numerical experiments were carried out to obtain insights about the parameter. In this study, a small number $\tilde{\varepsilon}$ is used in the range of $0.1 \leq \tilde{\varepsilon} \leq 1.0$, and solution accuracy was compared. Figure 3 is the resulting stagnation pressure history obtained with different $\tilde{\varepsilon}$ values. The larger values of the entropy fixing parameter represent the shift of pressure peaks to the left without a problem, just as the diffusive limiter function did. However, in case of the smallest number, $\tilde{\varepsilon} = 0.1$, the periodicity of solution breaks down after a long time. A larger value of entropy-fixing parameter cures this problem. Thus, it is concluded that a larger value of entropy-fixing parameter results in a diffusive solution, but can be used without significant deterioration if the solution stability is the biggest problem.

Application of an AUSM-Based Method

Instead of Roe's FDS,[7] a different kind of upwind scheme was tested in addition to the limiter functions and entropy fix. In this study, an AUSM+W (Ref. 9) flux-splitting method was considered with pressure limiter function.[20] Recently, AUSM-based methods[21] or AUSM-like methods[11] began to be used widely for the problems where stable shock capturing is a major concern and Roe's FDS fails due to the instability of the normal shock wave. However, the previous studies have shown that AUSM[21] has a problem of postshock oscillation when a strong shock wave is involved, and a number of its variants are developed to overcome this problem.[9,11,20] Thus, because AUSM methods are still under development, they should be validated for a sufficient number of applications. In this study, AUSM+W, an advanced version of AUSM, is applied with the combinations of MUSCL-minmod and MUSCL-pressure limiter. The pressure limiter has showed somewhat diffusive characteristics but is often used with the stiff AUSM method as a remedy for postshock oscillation problems that AUSM can have.[20]

Figure 4 is the solution provided by the AUSM+W with MUSCL-pressure limiter combination. In Mach number distribution, the reaction zone in the frontal subsonic region shows nearly steady characteristics whereas the old reaction front moves out downstream. In density variation, the oscillatory characteristics of the reaction front is maintained for one or two periods, but it ultimately disappears. This trend can be more easily seen in the pressure history in Fig. 5. The decaying of the oscillation is noticed in the results, whereas Roe's FDS method[7] and the MUSCL-minmod combination maintain the oscillation throughout the computing time. After about 2000 steps of time integration (at about 20 μs), the oscillation is completely eliminated, and the result shows steady-state behavior. This unphysical behavior may be a result of the diffusive shock-capturing characteristics of the MUSCL-pressure limiter combination. However, the MUSCL-minmod combination shows

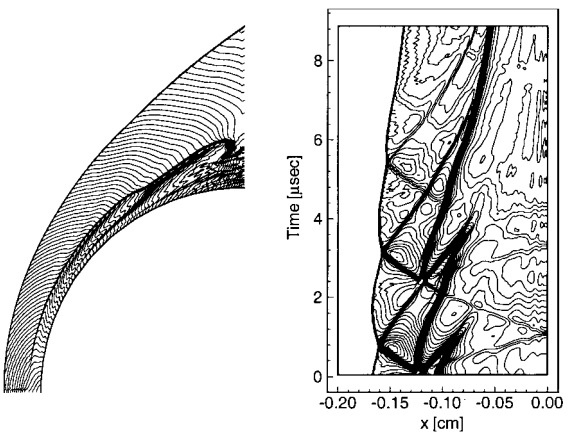

Fig. 4 Local Mach number distribution and the temporal variation of density along stagnation line for the case of $M = 4.48$ with AUSM+ and first-order time integration.

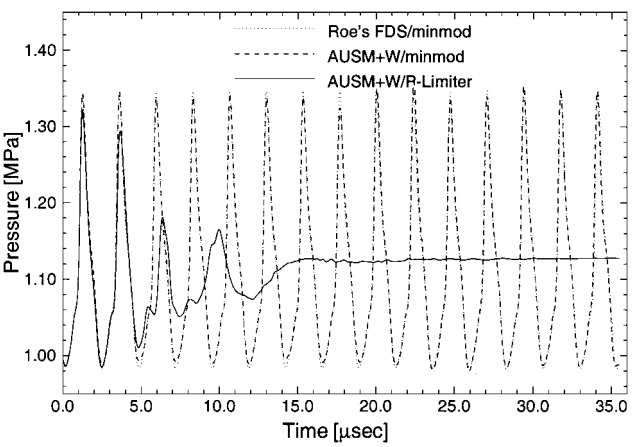

Fig. 5 Comparison of temporal variations of pressure at stagnation point for Roe's FDS and AUSM+W with minmod limiter and a pressure limiter for 4000 time steps.

nearly the same oscillation characteristics as Roe's FDS[7] except for the slightly lower maximum pressure and slightly higher minimum pressure.

Note that the selection of a shock-capturing scheme and its generic numerical diffusivity are very important for the correct simulation of unstable combustion phenomena because an inappropriate selection of spatial discretization schemes may result in a completely different result. Although the simple vector formulation makes the AUSM+W more efficient than Roe's FDS,[7] reduction of total computing time was insignificant due to the implicit formulation.

Comparison of Time-Integration Methods

Next, different time-integration schemes are compared with a time step refinement study to find the efficiency and the accuracy of the schemes for the unsteady shock-induced combustion problem. An explicit four-step RK method,[12] a PI method,[13] a fully implicit CN method,[12] and a dual-time-stepping method,[14] are considered in this study as representatives of various time-integration schemes.

Explicit Four-Step RK Method

It is generally known that an implicit scheme is more efficient than an explicit scheme due to time step limitations from stability restrictions of convection terms and the stiffness of chemistry terms. However, this is not always true for reactive flow simulations involving a large number of species conservation equations because, although an explicit treatment of a chemical source term requires that the numeric operations be proportional to the number of species, an implicit treatment of a chemistry Jacobian matrix requires that the operations be proportional to the cubic number of species. Thus, the efficiency of implicit schemes is degraded with the increase in the number of species. For the comparison of an explicit scheme to an implicit scheme, the standard fourth-order time-accurate four-step RK method was applied for an Euler equation of chemically reacting flow in Eq. (1):

$$\boldsymbol{Q}^{(1)} = \boldsymbol{Q}^n + \tfrac{1}{2}\Delta t \boldsymbol{R}^n, \qquad \boldsymbol{Q}^{(2)} = \boldsymbol{Q}^n + \tfrac{1}{2}\Delta t \boldsymbol{R}^{(1)}$$

$$\boldsymbol{Q}^{(3)} = \boldsymbol{Q}^n + \Delta t \boldsymbol{R}^{(2)}$$

$$\boldsymbol{Q}^{n+1} = \boldsymbol{Q}^n + (\Delta t/6)\left(\boldsymbol{R}^n + 2\boldsymbol{R}^{(1)} + 2\boldsymbol{R}^{(2)} + \boldsymbol{R}^{(3)}\right) \qquad (6)$$

Spatial discretization in the residual vector is the same as in the baseline method. The stability limit of this scheme is known as Courant–Friedrichs–Lewy (CFL) number of $2\sqrt{2}$ for convection equations, but it does not apply to a reactive flow system having stiff chemistry source terms. Residual term $\boldsymbol{R}$ is evaluated by Eq. (3) at each substep by using the intermediate values of conservative variables. Even with the four-step evaluation of the residual vector, a time step of RK needs less time than the implicit method because matrix inversion is not necessary.

Numerical experiments were performed with this method using time steps equivalent to CFL numbers of 0.3, 1.0, and 1.5. The first-order-accurate solution of the baseline method is used as an initial condition with all other conditions fixed to that used in the simulation of experimental results. Figure 6 is the stagnation pressure history using the RK method, and the magnified view of high-frequency oscillation is plotted in Fig. 7. The solutions of all of the cases show similar trends and the advantageous properties of this method, even with the large variation in CFL number. However, CFL numbers larger than 1.5 were not available, and the solution blew out. Thus, a CFL number of 1.5 seems to be a practical limit for the present simulation. This CFL number is considered sufficiently large considering its efficiency, even though we cannot guarantee its applicability to viscous problems, which are important in practical propulsion devices and which require very fine grids.

One step of time integration takes 11.19 s/iteration on a DEC Personal Workstation having a 500-MHz Alpha 21164 Microprocessor with 1 MB of L2 cache and 128 MB of main memory. This is an encouraging result compared with the time needed for the baseline method with two subiterations taking 34.24 s per iteration,[1] even after taking into account the twice-as-large number of iterations.

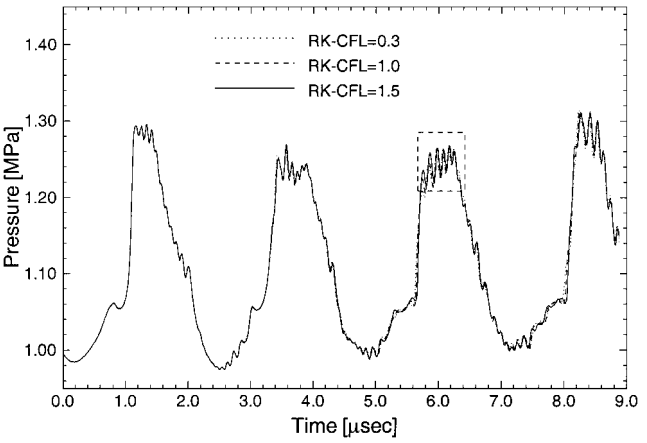

Fig. 6 Temporal variations of pressure at stagnation point by explicit four-step RK method with different time steps.

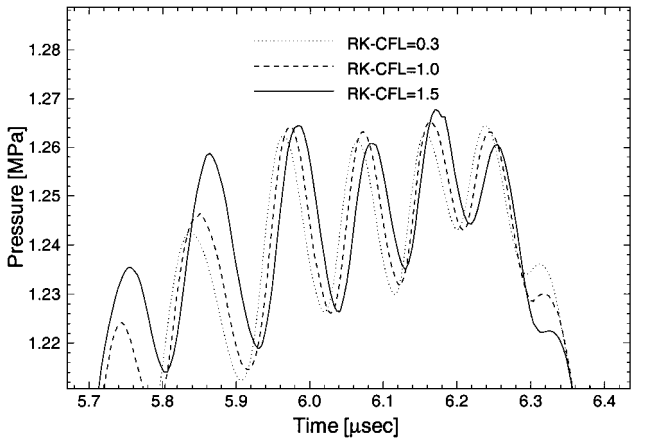

Fig. 7 Temporal variations of pressure at stagnation point by explicit four-step RK method with different time steps; magnified plot of dotted box in Fig. 6.

Thus, it is believed that the explicit RK method could be a powerful tool for multispecies reacting flow that includes a large number of partial differential equations, unless the time step size is limited by the coupling of the convection term and stiff chemical source terms.

PI Method

In a case where the stiffness of chemistry term is a problem, only the chemistry term is treated implicitly[2,11,13,22] to overcome the stiffness. Thus, the simplest form of a PI method is also considered in this study among the various formulations of PI or semi-implicit schemes.[6,22] Using the PI method of one-step time integration, Eq. (1) can be discretized as

$$(\boldsymbol{I}/\Delta t - \boldsymbol{Z})^n_{i,j}\Delta \boldsymbol{Q}^n_{i,j} = \boldsymbol{R}^n_{i,j}, \qquad \boldsymbol{Q}^{n+1}_{i,j} = \boldsymbol{Q}^n_{i,j} + \Delta \boldsymbol{Q}^n_{i,j} \qquad (7)$$

Figure 8 shows the temporal variations of pressure at the stagnation point using the PI method. In this approach, the CFL number ranges from 0.03 to 0.5. The results at large time steps show severe high-frequency oscillation that could not be considered a physical result. However, the amplitude of oscillation is mitigated and tends to converge to certain amplitudes using a small time step, although the period of the high-frequency oscillation is nearly unchanged. This trend is shown clearly in Fig. 9. From this time step refinement study, it is believed that the CFL number should be less than 0.1 for the analysis of the present problem, considering the solution quality compared with that of baseline method or that of the RK method. This limitation of time step size is a very severe restriction of the PI method, even though an iteration requiring one $N \times N$ matrix inversion takes only 7.04 s/iteration.

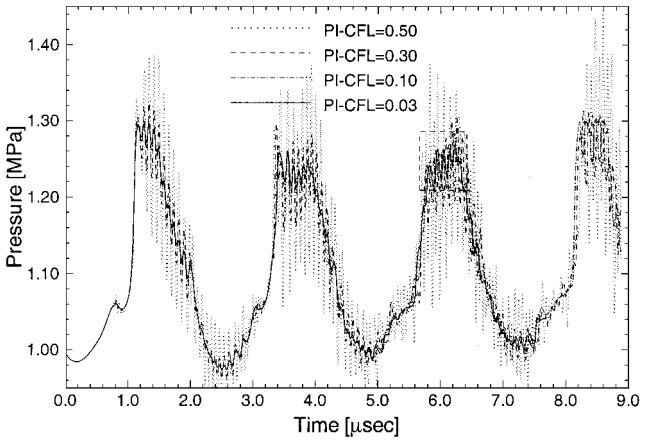

Fig. 8 Temporal variations of pressure at stagnation point by PI method with different time steps.

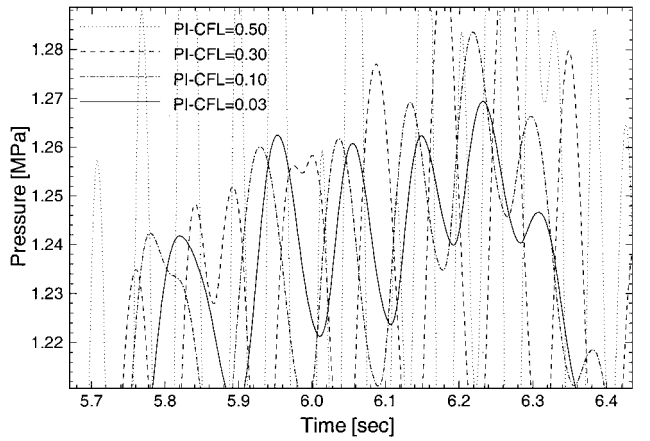

Fig. 9 Temporal variations of pressure at stagnation point by PI method with different time steps; magnified plot of dotted box in Fig. 8.

CN Method

The simplest form of second-order time-accurate fully implicit method is a CN method, in which only one-half of a Jacobian matrix of residual terms is considered. By applying the CN method, the governing equations can be discretized as

$$\left(\frac{\boldsymbol{I}}{\Delta t}-\frac{1}{2}\left(\frac{\partial \boldsymbol{R}}{\partial \boldsymbol{Q}}\right)\right)^{n}_{i,j}\Delta \boldsymbol{Q}^{n}_{i,j}=\boldsymbol{R}^{n}_{i,j},\qquad \boldsymbol{Q}^{n+1}_{i,j}=\boldsymbol{Q}^{n}_{i,j}+\Delta \boldsymbol{Q}^{n}_{i,j} \tag{8}$$

The baseline method can be modified as a CN method in Eq. (8) simply by replacing the time step coefficient as

$$c_0=2/\Delta t^{n},\qquad c_1=-c_0,\qquad c_2=0 \tag{9}$$

Figure 10 is the summarized result of CN method with a CFL number ranging from 0.3 to 3.0. These solutions also show high-frequency oscillations, but the solution also converges to a solution with small amplitude when small time steps are used. This converging trend is more clearly understood from Fig. 11. The oscillation of the nearly converged solution seems to have nearly the same frequency and amplitude as those derived from the RK method and PI method. From this examination, it is believed that the CFL number should be less than 1.0 for the CN method because it shows a stability problem of high-frequency oscillation at large time steps. Nevertheless, the efficiency of CN method with CFL number of 1.0 can be compared to the baseline method with two subiterations while using a CFL number of 3 because the computation time for an iteration of the CN method is almost the same as that of the baseline method without a subiteration.

Baseline Newton Subiteration Method

The time step refinement study is also carried out for the present baseline method with CFL number ranging from 0.3 to 6.0. The result of the time step refinement study for the subiteration method is plotted in Figs. 12 and 13. A subiteration convergence criterion of 1% error was used in this study rather than the restriction of a maximum subiteration number of 4, such as was used in the simulation of experiments.[1] With this convergence criterion, about five subiterations are needed in most of the integration steps for the case of CFL number of 6 to satisfy the convergence criterion, less than two subiterations for a CFL number of 1.0, and no subiteration for a CFL number of 0.3.

This result says that the efficiency increase is not proportional to the increase of time step size because many subiterations are needed

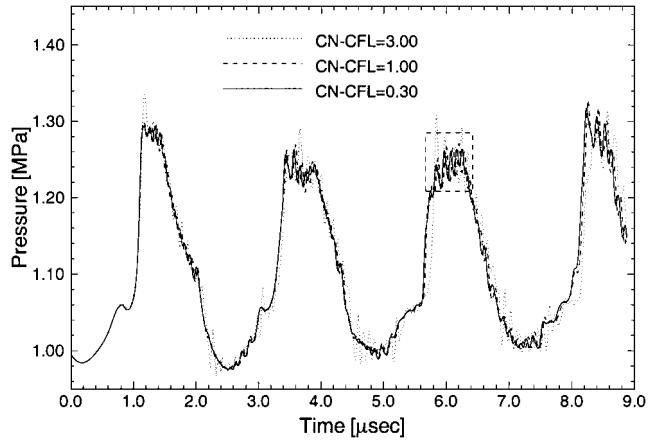

Fig. 10 Temporal variations of pressure at stagnation point by CN method with different time steps.

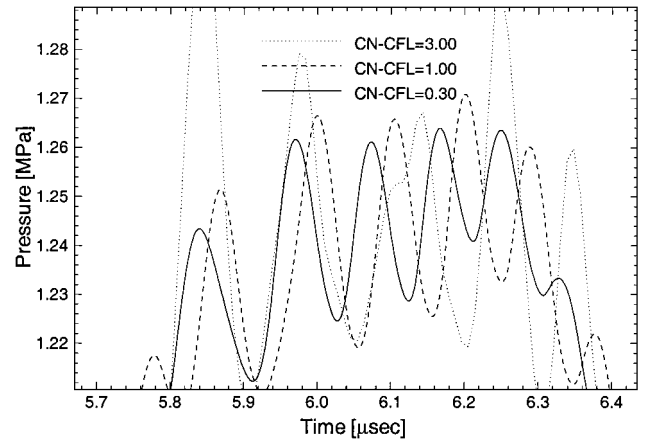

Fig. 11 Temporal variations of pressure at stagnation point by CN method with different time steps; magnified plot of dotted box in Fig. 10.

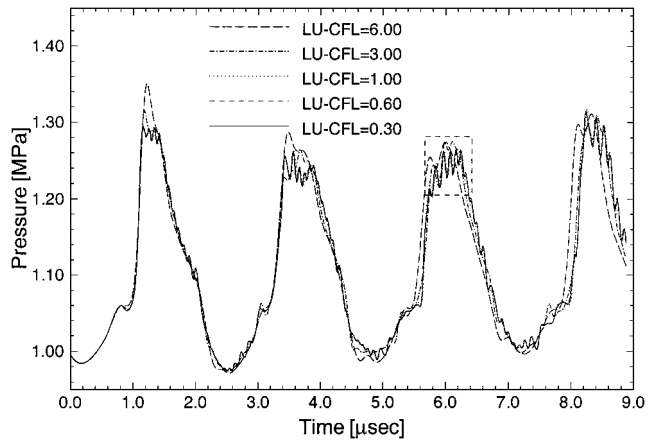

Fig. 12 Temporal variations of pressure at stagnation point by LU symmetric Gauss–Seidel scheme with different time steps.

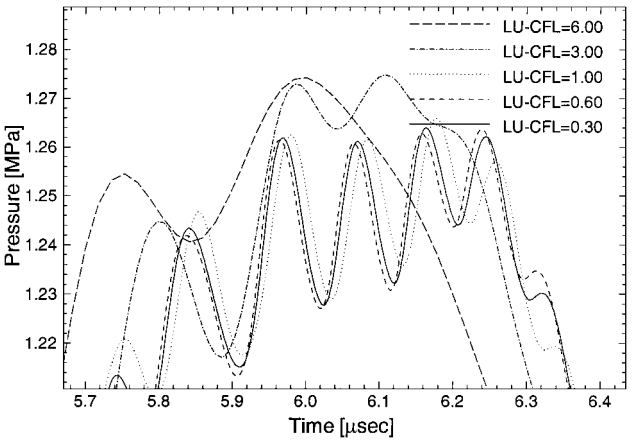

Fig. 13 Temporal variations of pressure at stagnation point by LU-SGS method with different time steps; magnified plot of dotted box in Fig. 12.

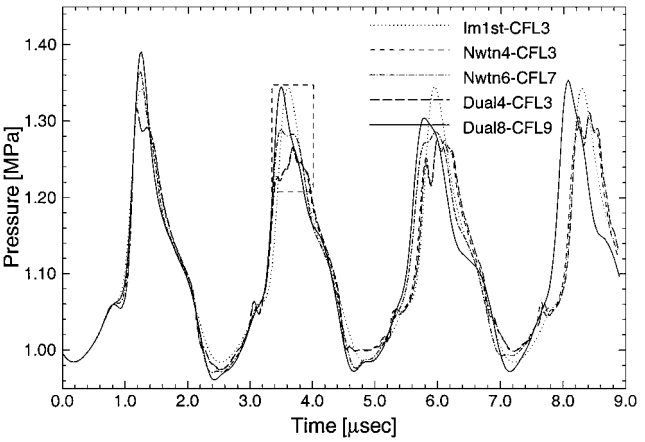

Fig. 14 Comparison of temporal pressure variations at stagnation point using Newton subiteration method and dual-time-stepping method.

for convergence at a large time step. Even with this mitigation of efficiency increase, the solution with a large time step seems to be desirable because the solution does not show a high-frequency oscillation and looks stable. Thus, the solution stability of the baseline method is comparable to the PI method or the CN method, both of which have severe oscillation problems with large time step size. However, there is an actual limitation of time step size for this subiteration approach. A slight phase shift is noticed for the case of a CFL number of 6.0 and a much larger time step showed solution failure even with the much larger number of subiterations. On the other hand, Fig. 13 also shows the high-frequency, small-amplitude oscillation of the baseline method for small time steps, and the solution shows the converging trend similar to that for the RK method, the PI method, and the CN method as shown in Fig. 13.

Dual-Time-Stepping Method

Another type of subiteration method is the dual-time-stepping method. In this method, a pseudo-time derivative is assumed and included in the left-hand side of governing equation (1):

$$\frac{\partial \boldsymbol{Q}}{\partial \tau} + \frac{\partial \boldsymbol{Q}}{\partial t} + \frac{\partial \boldsymbol{F}}{\partial \xi} + \frac{\partial \boldsymbol{G}}{\partial \eta} + \boldsymbol{H} = \boldsymbol{W} \tag{10}$$

This pseudo-time derivative is considered only for iteration purposes at every time step only to find the solution satisfying Eq. (1). In this scheme, the physical time derivative is discretized in first- or second-order-accurate form, as was done in the baseline method, at every time increment step. The discretized form of this method is very similar to the Newton subiteration method in Eq. (2) except for the inclusion of $1/\Delta\tau$ in the diagonal part of left-side matrix, although the basic concept of subiteration is different. Thus, the dual-time-stepping method is equivalent to the Newton subiteration scheme at the limit of infinite pseudo-time step:

$$\left(\left(\frac{1}{\Delta\tau} + c_0\right)\boldsymbol{I} - \left(\frac{\partial \boldsymbol{R}}{\partial \boldsymbol{Q}}\right)\right)_{i,j}^{n+1,m} \Delta \boldsymbol{Q}_{i,j}^{n+1,m}$$

$$= -c_0 \boldsymbol{Q}_{i,j}^{n+1,m} - c_1 \boldsymbol{Q}_{i,j}^{n} - c_2 \boldsymbol{Q}_{i,j}^{n-1} + \boldsymbol{R}\left(\boldsymbol{Q}_{i,j}^{n+1,m}\right) \tag{11}$$

The presence of a pseudo-time derivative enforces the diagonal dominance of the scheme, makes the solution much more stable, and permits a larger time step than in the Newton subiteration scheme. In the present study, the pseudo-time step is selected as equal to the physical time step. Figures 14 and 15 are the solutions of stagnation pressure history compared with that of the Newton subiteration scheme. Because efficiency is the major purpose of this scheme, tests were done only with large time steps. With the same physical time step of a CFL number of 3.0 and the same iteration number of 4, the solution of the dual-time-stepping scheme seems nearly the same as that of Newton subiteration scheme. For the Newton subiteration scheme, a CFL number of 7.0 was a practical maximum value of time step without solution failure, and six iterations

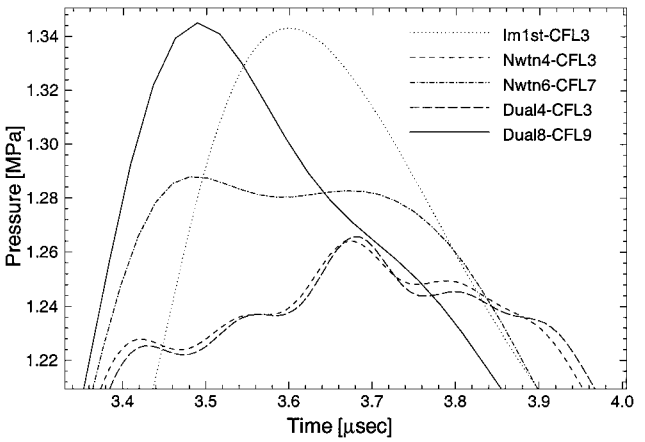

Fig. 15 Comparison of temporal pressure variations at stagnation point using Newton subiteration method and dual-time-stepping method; magnified plot of dotted box in Fig. 14.

were needed to meet the 1% convergence criterion. In the case of the dual-time-stepping method, a CFL number of 9.0 was possible, but the seven subiterations degrade the effectiveness of this scheme. Moreover, the solutions at larger time steps show a very diffusive solution that is very similar to the first-order time-accurate solution. Thus, the large time step should be avoided for the sake of solution accuracy even though the large time step can be used without solution blowout or divergence.

Comparison of Time-Integration Methods

For the comparison of the converging trends, the solutions from the aforementioned integration methods with smallest time step cases are summarized in Figs. 16 and 17. The four solutions show nearly the same pressure histories with high-frequency small-amplitude oscillations. The oscillatory solution is considered reliable because the results from the different methods show nearly the same converging solution at small time steps. The high-oscillation frequency shown in Fig. 16 is about 12 MHz. However, it is unclear if the high-frequency oscillation is a physical one or a numerical one originating from the nonlinear shock capturing scheme because such a high-frequency oscillation has not been observed in previous studies (although it is a converged solution with small time step size). The computing time, a period equivalent to 1000 iterations of the baseline method with a CFL number if 3.0, is listed in Table 2 for comparison of the solution effectiveness of each time-integration method. In Table 2, time/iteration is measured from 100 iterations of each method on a DEC Personal Workstation and used for the estimation of wall clock time. This was done because the calculations in the present study were carried out using several different machines having different performances. In Table 2, the explicit four-step RK method

Table 2 Comparison of solution effectiveness of time-integration methods for a period equivalent to 1000 iterations of the baseline Newton subiteration method

CFL	Iterations	Time/ iteration, s	Wall clock time, s	Comments on effectiveness
			RK	
0.3	10,000	11.19	111,900	——
1.5	2,000	11.19	22,380	Good, largest CFL number available
			PI	
0.1	30,000	7.04	211,200	——
0.3	10,000	7.04	70,400	Bad, largest CFL number tolerable
			CN	
0.3	10,000	12.81	128,100	——
1.0	3,000	12.81	38,400	Good, largest CFL number tolerable
			Newton iteration	
0.3	10,000	12.81	128,100	No subiteration
3.0	1,000	35.66	35,660	Baseline solution, about two subiterations
6.0	500	71.28	35,640	Phase shift, about five subiterations
			Dual time stepping	
9.0	333	102.5	34,167	Phase shift about seven subiterations

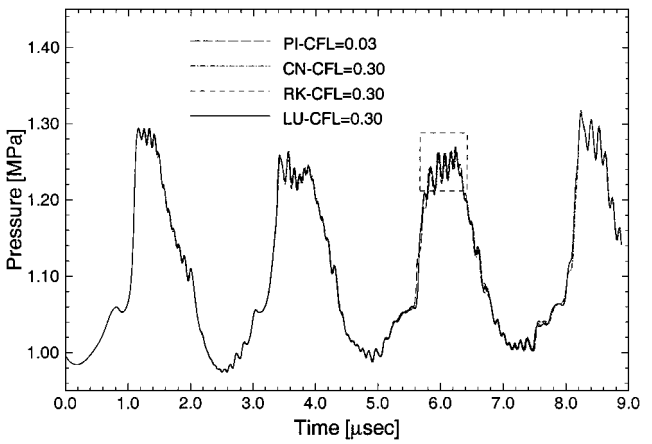

Fig. 16 Comparison of temporal variations of pressure at stagnation point from different time-integration methods.

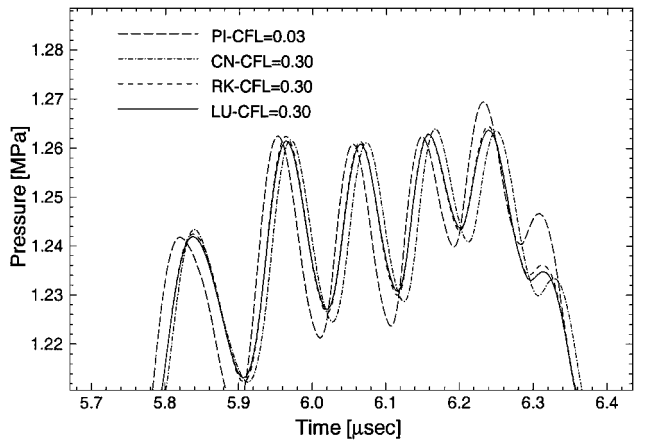

Fig. 17 Comparison of temporal variations of pressure at stagnation point from different time-integration methods; magnified plot of dotted box in Fig. 16.

shows the best performance regardless of limited CFL number; however, this method needs more verification for the problems involving the strong coupling of convection and chemistry or shock and viscous interactions. Single-step PI schemes have severe restrictions on time step size even with the implicit treatment of chemistry terms. The CN method shows relatively good performance considering its simple formulation and second-order time accuracy. The efficiencies of two subiteration methods were nearly the same, but the dual-time-stepping method was more stable and permits a large time step. However, the solution quality of fully implicit formulation at a large CFL number is not guaranteed due to the diffusive character of these schemes. Also, the solution efficiency was not improved greatly at a large CFL number due to the increased number of subiterations for convergence. Thus, it was found that there is a practical limit of time steps for these subiteration schemes, considering the efficiency and solution quality. In this study, the practical limit is considered to be a CFL number of about 3.0.

Conclusions

A comparative study of numerical methods is made as part of the process of developing an efficient computational fluid dynamics code for unsteady reactive flows. As a baseline method, an iterative fully implicit algorithm is used for time integration, and a third-order-accurate upwind scheme is used for spatial discretization. The numerical experiment of spatial discretization methods and time-integration methods present some important points that should be taken into account in the analysis of these kinds of unsteady problems.

With regards to spatial discretization, the choice of different spatial limiter functions was compared. Comparison shows different frequencies in the range from 421.78 to 429.48 kHz, which is also in the range of the experimental results. A diffusive limiter resulted in a high-frequency oscillation and the stiff limiter resulted in small one, although the maximum deviation is limited to 2.5%. A test of entropy-fixing parameters reveals that a large value of entropy fix results in a diffusive solution but that they can be used without significant deterioration if the solution stability is a problem. The combination of the AUSM+W method with minmod limiter function results in nearly the same solution as the baseline method, but the combination with the pressure limiter function showed that a diffusive method might result in a completely different solution to the physical situation. Note from these studies that spatial discretization schemes should be selected very cautiously, to capture correctly the unsteady characteristics of shock-induced combustion because the numerical dissipation inherently contained in upwind schemes and limiter functions has an important role on the solution frequency.

A time step refinement study was carried out for different time-integration methods to find the time accuracy and solution efficiency of each scheme. In this study all of the methods show converged pressure histories using small time step sizes, and all of the methods show nearly the same pressure history, having small-amplitude, high-frequency oscillations overlaid on the basic large-amplitude, low-frequency oscillation. Even though the high-frequency oscillation cannot be assumed to be either a physical one or a numerical one at present, it is considered a numerically correct solution because all of the different time-integration methods using small time steps results in a single converged solution. With regard to the solution efficiency, both the RK method and the CN method can be good and simple substitutes of the baseline method, with reasonable efficiency even with the time step limitation, provided the second-order-accurate solution is really required. However, the CN method and the PI method using large time steps result in highly oscillatory solutions that cannot be accepted as solutions. The dual-time-stepping method and the baseline Newton subiteration method show nearly the same efficiency and solution quality with reasonable time step size. Even though the dual-time-stepping method was more stable and permits a large time step size, the fully implicit formulations with large time step result in a diffusive solution with a phase shift and the smearing of high-frequency oscillations. Moreover, a large time step size did not improve the solution efficiency due to the increase in subiterations for convergence. Therefore, it is believed that the greatest merit of the subiteration schemes is the large stability

limit, although there is a practical limit regarding time steps for these schemes when one considers the efficiency and the solution quality.

Acknowledgments

This research is supported by the Turbo and Power Machinery Research Center and the Korea Science and Engineering Foundation under Grant 971-1005-031-2.

References

[1]Choi, J. Y., Jeung, I.-S., and Yoon, Y., "Computational Fluid Dynamics Algorithms for Unsteady Shock-Induced Combustion, Part 1: Validation," *AIAA Journal*, Vol. 38, No. 7, 2000, pp. 1179–1187.

[2]Wilson, G. J., and Sussman, M. A., "Computation of Unsteady Shock-Induced Combustion Using Logarithmic Species Conservation Equations," *AIAA Journal*, Vol. 31, No. 2, 1993, pp. 294–301.

[3]Matsuo, A., Fujii, K., and Fujiwara, T., "Flow Features of Shock-Induced Combustion Around Projectile Traveling at Hypervelocities," *AIAA Journal*, Vol. 33, No. 6, 1995, pp. 1056–1063.

[4]Ahuja, J. K., Kumar, A., Singh, D. J., and Tiwari, S. N., "Simulation of Shock-Induced Combustion Past Blunt Projectiles Using Shock-Fitting Technique," *Journal of Propulsion and Power*, Vol. 12, No. 3, 1996, pp. 518–526.

[5]Yungster, S., and Radhakrishnan, K., "A Fully Implicit Time-Accurate Method for Hypersonic Combustion: Application to Shock-Induced Combustion Instability," AIAA Paper 94-2965, June 1994.

[6]Yee, H. C., "A Class of High Resolution Explicit and Implicit Shock-Capturing Methods," NASA TM-101088, Feb. 1989.

[7]Roe, P. L., "Approximate Riemann Solvers, Parameter Vectors, and Difference Schemes," *Journal of Computational Physics*, Vol. 43, 1981, pp. 357–372.

[8]Saxena, S. K., and Ravi, K., "Some Aspects of High-Speed Blunt Body Flow Computations with Roe Scheme," *AIAA Journal*, Vol. 33, No. 6, 1995, pp. 1025–1031.

[9]Liou, M.-S., "Progress Towards an Improved Computational Fluid Dynamics Method: AUSM+," AIAA Paper 95-1701, 1995.

[10]Choi, J.-Y., Jeung, I.-S., and Lee, S., "Dimensional Analysis of the Effect of Flow Conditions on Shock-Induced Combustion," *Twenty-Sixth Symposium (International) on Combustion*, Combustion Inst., Pittsburgh, PA, 1996, pp. 2957–2963.

[11]Sheffer, S. G., Jameson, A., and Martinelli, L., "Parallel Computation of Supersonic Reactive Flows with Detailed Chemistry," AIAA Paper 98-0899, Jan. 1998.

[12]Hirsch, C., *Numerical Computation of Internal and External Flows*, Wiley, New York, 1990.

[13]Choi, J.-Y., Jeung, I.-S., and Yoon, Y., "Numerical Study of Scram-Accelerator Starting Characteristics," *AIAA Journal*, Vol. 36, No. 6, 1998, pp. 1029–1038.

[14]Arnone, A., Liou, M.-S., and Povinelli, L. A., "Integration of Navier–Stokes Equations Using Dual Time Stepping and a Multigrid Method," *AIAA Journal*, Vol. 33, No. 6, 1995, pp. 985–990.

[15]Shuen, S., and Yoon, S., "Numerical Study of Chemically Reacting Flows Using a Lower–Upper Symmetric Successive Overrelaxation Scheme," *AIAA Journal*, Vol. 27, No. 12, 1989, pp. 1752–1760.

[16]Lehr, H. F., "Experiment on Shock-Induced Combustion," *Astronautica Acta*, Vol. 17, Nos. 4 and 5, 1972, pp. 589–597.

[17]Chen, C. L., McCroskey, W. J., and Obayashi, S., "Numerical Solution of Forward-Flight Rotor Flow Using an Upwind Method," *Journal of Aircraft*, Vol. 28, No. 6, 1990, pp. 374–380.

[18]Anderson, W. K., Thomas, J. L., and Van Leer, B., "Comparison of Finite Volume Flux Vector Splittings for the Euler Equations," *AIAA Journal*, Vol. 24, No. 9, 1986, pp. 1453–1460.

[19]Montagne, J. L., Yee, H. C., Klopfer, G. H., and Vinokur, M., "Hypersonic Blunt Body Computation Including Real Gas Effects," NASA TM 10074, March 1988.

[20]Edwards, J. R., "Low-Diffusion Flux-Splitting Schemes for Navier–Stokes Calculations," AIAA Paper 95-1713, 1995.

[21]Liou, M. S., and Steffen, C. J., "A New Flux Splitting Scheme," *Journal of Computational Physics*, Vol. 1079, 1993, pp. 23–39.

[22]Bussing, T. R. A., and Murman, E. M., "Finite Volume Method for the Calculation of Compressible Chemically Reacting Flows," *AIAA Journal*, Vol. 26, No. 9, 1988, pp. 1070–1078.

K. Kailasanath
Associate Editor